Chloroquine drug and Graphene complex for treatment of COVID-19

Saeedeh Mohammadi
Department of Physics, Azarbaijan Shahid Madani University, Tabriz, Iran
Mohammad Esmailpour (Esmailpour@azaruniv.ac.ir)
Department of Physics, Azarbaijan Shahid Madani University, Tabriz, Iran
Mina Mohammadi
Department of Pharmaceutical Biomaterial, School of Pharmacy, Zanjan University of Medical Sciences, 56184-45139, Zanjan, Iran

Research Article

Keywords: COVID-19, chloroquine graphene complex, structural and electrical properties, absorption, density functional theory (DFT) method

Posted Date: May 15th, 2020

DOI: https://doi.org/10.21203/rs.3.rs-29418/v1

Chloroquine drug and Graphene complex for treatment of COVID-19

Saeedeh Mohammadi[1], Mohammad Esmailpour[1,*], and Mina Mohammadi[2]

[1]Department of Physics, Azarbaijan Shahid Madani University, Tabriz, Iran
[2]Department of Pharmaceutical Biomaterial, School of Pharmacy, Zanjan University of Medical Sciences, 56184-45139, Zanjan, Iran
[*]Esmailpour@azaruniv.ac.ir

ABSTRACT

This paper is a new step in helping the treatment of coronavirus by improving the performance of chloroquine drug. For this purpose, we propose a complex of chloroquine drug with graphene nanoribbon (GNR) scheme. We compute the structural and electrical properties and absorption of chloroquine ($C_{18}H_{26}ClN_3$) and GNR complex using the density functional theory (DFT) method. By creating a drug and GNR complex, the density of states of electrons increases and the energy gap decreases compared to the chloroquine. Also, using absorption calculations and spectrums such as infrared and UV-Vis spectra, we showed that GNR is a suitable structure for creating chloroquine drug complex. Our results show that the dipole moment, global softness and electrophilicity for the drug complex increases compared to the non-complex state. Our calculations can be useful for increasing performance and reducing the side effects of chloroquine, and thus can be effective in treating coronavirus.

Introduction

In the end of 2019, in China, a virus similar to human coronaviruses, SARS and MERS[1–4] pneumonia, was reported, later called COVID-19[5,6]. According to the World Health Organization (WHO), in April 2020, more than 2 million cases of the virus and about 150,000 deaths were reported[7]. Recently, with the appearance and increase of coronavirus epidemic in many countries, chloroquine has become a major drug in the treatment of coronavirus.[8–11]. In the past years, chloroquine drug was used to therapy and control of malaria[8,11,12]. Recent studies have shown that this drug successfully treats patients with coronavirus pneumonia[11]. Also, the chloroquine drug has potential applications in the treatment of diseases such as rheumatoid arthritis (RA)[13], systemic lupus erythematosus (SLE)[14–16], antiphospholipid syndrome (APS)[17] and primary Sjogren syndrome[18]. Previous studies have shown that chloroquine has an antiviral mechanism and by increasing the pH, it prevents unwanted viruses such as human immunodeficiency virus (HIV)[19], Zika virus[20,21], Ebola virus[22] and the avian leucosis virus[23] from entering the cell. Also, chloroquine can prevent the virus gene from multiplying by increasing the pH[24,25]. To increase the effectiveness of chloroquine and to increase special cellular uptake and reduce nonspecific gathering in the vivo tissues, the design of drug delivery systems for chloroquine drug is required. The drug delivery systems can control the drug release in vivo and increase performance encapsulation and absorption[26,27]. Nanomaterial-based drug delivery systems have $\pi-\pi$ stacking interactions or covalent crosslinking with drug molecules due to their small size[28–31]. Graphene, as a member of nanomaterials with a two-dimensional structure with strong $\pi-\pi$ stacking bond[32], has unique physical, chemical and optical properties. For this reason, graphene was noticed in biomedical issues such as drug delivery[33–35] and biosensors[36,37]. This drug is consumed orally and absorbed in most vivo tissues which increases side effects and reduces the performance of the chloroquine in lung tissue. But by combining this drug, the possibility of passing through every tissue is reduced. Therefore, the side effects of the drug are reduced and the effectiveness of the drug in the vivo tissues is increased. Any previous research on chloroquine and GNR complex has not been performed. Therefore, a study of the electrical and structural properties of chloroquine with graphene is essential for drug delivery vivo. In this paper, we theoretically examine the absorption and electrical and structural properties of chloroquine attached to graphene nanoribbon (GNR), which has potential applications in drug delivery.

1 Model and Method

We investigate the structural and electrical properties of a system including chloroquine drug, with the chemical formula $C_{18}H_{26}ClN_3$ and the IUPAC name $N'-(7-chloroquinolin-4-yl)-N,N-diethyl-pentane-1,4-diamine$, and GNR that is connected to hydrogen atoms from the edges (as shown in Figure 1). Figs. 1 (a), (b) and (c) show this structure from the side and up view schematically and Fig. 1(d) shows a part of the connection between GNR and chloroquine. Our calculations

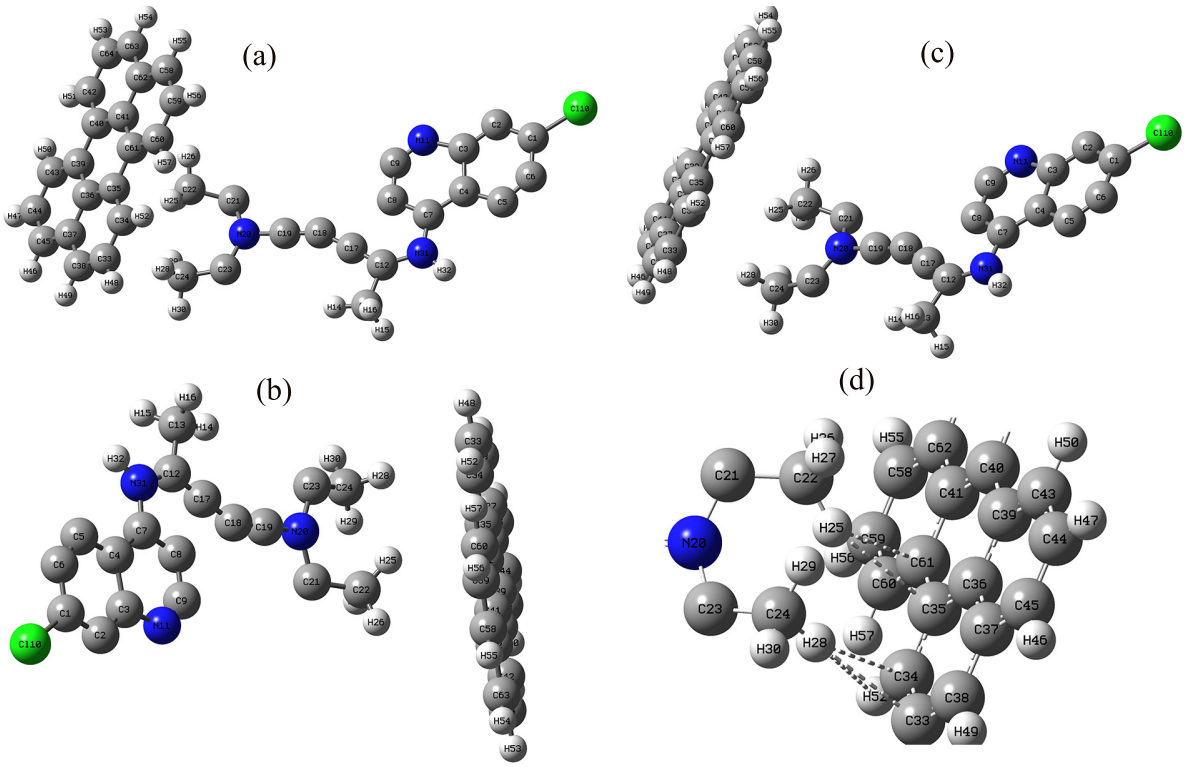

Figure 1. Three-dimensional view of the complex of chloroquine and GNR from different views (the sharp of (a), (b) and (c)) and the part of intraction between chloroquine and GNR (d).

are based on the density functional theory (DFT) and were performed by using Gaussian 09 (G09) program package[38]. In this work, the exchange and correlation energy function is performed by applying the B3LYP method in G09[39,40]. To study the electrical and structural properties of the system, we use the 3-21 g basis set[41,42]. In Ref. 43, good results have been obtained by B3LYP method with long-range correlations. Using the results of the frequency calculations and optimized structures, we determined the absorption energy for chloroquine-GNR complex. Then, we calculated the electronic properties of chloroquine and GNR. We introduced E_{LOMO}, the lowest unoccupied molecular orbital (LUMO) energy, and E_{HOMO}, the highest occupied molecular orbital (HOMO) energy, defined as $E_{gap} = E_{LUMO} - E_{HOMO}$ and $E_F = (E_{LUMO} + E_{HOMO})/2$[44] in which E_{gap} and E_F are the energy gap and Fermi energy respectively (all listed in Table 1).

We describe another parameters such as: the chemical potential (μ), chemical hardness (η), global softness (S) and electrophilicity index (ω), which may be written as[45]:

$$\mu = \frac{(E_{HOMO} + E_{LUMO})}{2}. \tag{1}$$

$$IP = -E_{HOMO}, \tag{2}$$

$$EA = -E_{LUMO}. \tag{3}$$

$$\eta = \frac{(E_{HOMO} - E_{LUMO})}{2}, \tag{4}$$

$$S = \frac{1}{\eta}. \tag{5}$$

$$\omega = \frac{\mu^2}{2\eta}. \tag{6}$$

Absorption energy can be obtained using the following relations[45,46]:

$$E_{abs} = E_{G-D} - (E_G + E_D). \tag{7}$$

where E_G, E_D and E_{G-D} are GNR energy, the drug molecule energy and chloroquine-GNR complex energy respectively.

2 Results and discussion

In this section, we study the electron density of states, IR and UV- Vis spectrums in optimized GNR structures, chloroquine and complex of chloroquine-GNR. We considered GNR and chloroquine drug with the chemical formula of $C_{20}H_{12}$ and $C_{18}H_{26}ClN_3$ respectively. Our calculations show that the best position of chloroquine drug to interact with GNR is N-terminal of drug (Figure 1), because the energy of absorption is almost the same as the amount of energy absorbed by applying the counterpoise correction.

We obtained the optimized geometrical structures of the drug, GNR and complex of chloroquine-GNR. The bond length of atoms of chloroquine drug and chloroquine-GNR nanostructures are explained in the Table 1.

2.0.1 Chloroquine drug

The bond length of atoms $C-C$, $C-H$ and $C-N$ are equal to $1.2-1.53$, $1.09-1.1$, $1.19-1.44$ $(\overset{o}{A})$ respectively. The bond angles of atoms obtained for $C-C-C$, $C-N-C$ and $C-N-H$ are 112.5°-177.9°, 111.2°-134.7° and 106.4°-111.2° respectively. We also obtained the bond length of $Cl-C$ equal to 1.84 $(\overset{o}{A})$ and the bond angle for $Cl-C-C$ equal to 124.9°.

2.0.2 GNR

Now, we consider a finite-sized GNR whose edges are attached to hydrogen atoms. Optimized GNR shows that the bond lengths of $C-C$ and $C-H$ atoms are 1.37-1.48 $(\overset{o}{A})$ and 1.081-10.84 $(\overset{o}{A})$ respectively. The bond angles of $C-C-H$ atoms are from 118.7° to 120.1° and for $C-C-C$ atoms from 118.6° to 121.8°.

2.0.3 Chloroquine-GNR Complex

In this section, we obtained the structural properties of the complex chloroquine drug and GNR. Table 1 shows the bond length of the $C-C$, $C-H$ and $C-N$ atoms from 1.20 to 1.53 $(\overset{o}{A})$, 1.09 to 1.10 $(\overset{o}{A})$ and 1.19 to 1.44 $(\overset{o}{A})$ respectively. The bond angles of $C-C-C$, $C-N-C$ and $C-N-H$ atoms are 112.6°-178.2°, 111.2°-134.4° and 108.1°-118.9° respectively. In $C-Cl$, the bond length is 1.84 $(\overset{o}{A})$ and the bond angle of $C-Cl-C$ atoms is 122.4°. Table 1, shows that the bond length of atoms like $C-Cl$, $C-N$, $N-H$, $C-C$ and $C-H$ in the chloroquine and GNR complex is slightly reduced compared to the chloroquine itself. For the complex, in the chloroquine-GNR interaction zone, the bond length of the atoms is between 2.74 $(\overset{o}{A})$ and 3.50 $(\overset{o}{A})$, the details of which are listed in Table 2.

2.1 Electronic properties

In this section, we are going to describe the electrical properties of the mentioned system. The density of state (DOS) versus the incident electron energy are shown in Figure 2 using the GaussSum 3.0.2 program for GNR, chloroquine and chloroquine-GNR complex. Figure 2 shows that for GNR there is a large energy gap between HOMO and LUMO, while for chloroquine the energy gap is smaller than that of GNR. Clearly, the DOS is very highlighted in the vicinity of Fermi energy in chloroquine drug. As it is shown, the sharpness of peaks in GNR is reduced compared to the drug. DOS for GNR has also increased compared to drug. Thus, electron conductance for chloroquine has decreased. The energy gap of the drug and GNR complex is reduced compared to the drug and GNR. But the electron conductance in the drug and GNR complex is increased in comparison to the GNR and chloroquine. Also in DOS profiles the sharpness of peaks, in chloroquine-GNR complex, are highlighted compared to GNR.

Atoms	Chloroquine	Chloroquine-GNR
$C_1 - C_6$	1.382	1.382
$C_1 - C_2$	1.367	1.367
$C_1 - Cl$	1.845	1.848
$C_2 - C_3$	1.354	1.355
$C_5 - C_6$	1.268	1.268
$C_4 - C_5$	1.391	1.391
$C_3 - C_4$	1.532	1.533
$C_3 - N_{11}$	1.449	1.449
$C_9 - N_{11}$	1.196	1.196
$C_8 - C_9$	1.38	1.379
$C_7 - C_8$	1.437	1.438
$C_4 - C_7$	1.420	1.421
$C_7 - N_{31}$	1.370	1.369
$H_{32} - N_{31}$	1.014	1.014
$N_{31} - C_{12}$	1.394	1.395
$C_{12} - C_{13}$	1.493	1.493
$C_{13} - H_{14}$	1.092	1.092
$C_{13} - H_{15}$	1.097	1.097
$C_{12} - C_{17}$	1.393	1.393
$C_{17} - C_{18}$	1.405	1.405
$C_{18} - C_{19}$	1.205	1.205
$C_{19} - N_{20}$	1.375	1.377
$N_{20} - C_{23}$	1.409	1.417
$N_{20} - C_{21}$	1.441	1.438
$C_{23} - C_{24}$	1.513	1.507
$C_{24} - H_{29}$	1.093	1.093
$C_{24} - H_{28}$	1.103	1.096
$C_{24} - H_{30}$	1.096	1.096
$C_{21} - C_{22}$	1.504	1.502
$C_{22} - H_{25}$	1.093	1.091
$C_{22} - H_{27}$	1.103	1.104
$C_{22} - H_{26}$	1.099	1.098

Table 1. The bond length of the optimized chloroquine and drug-GNR complex atoms.

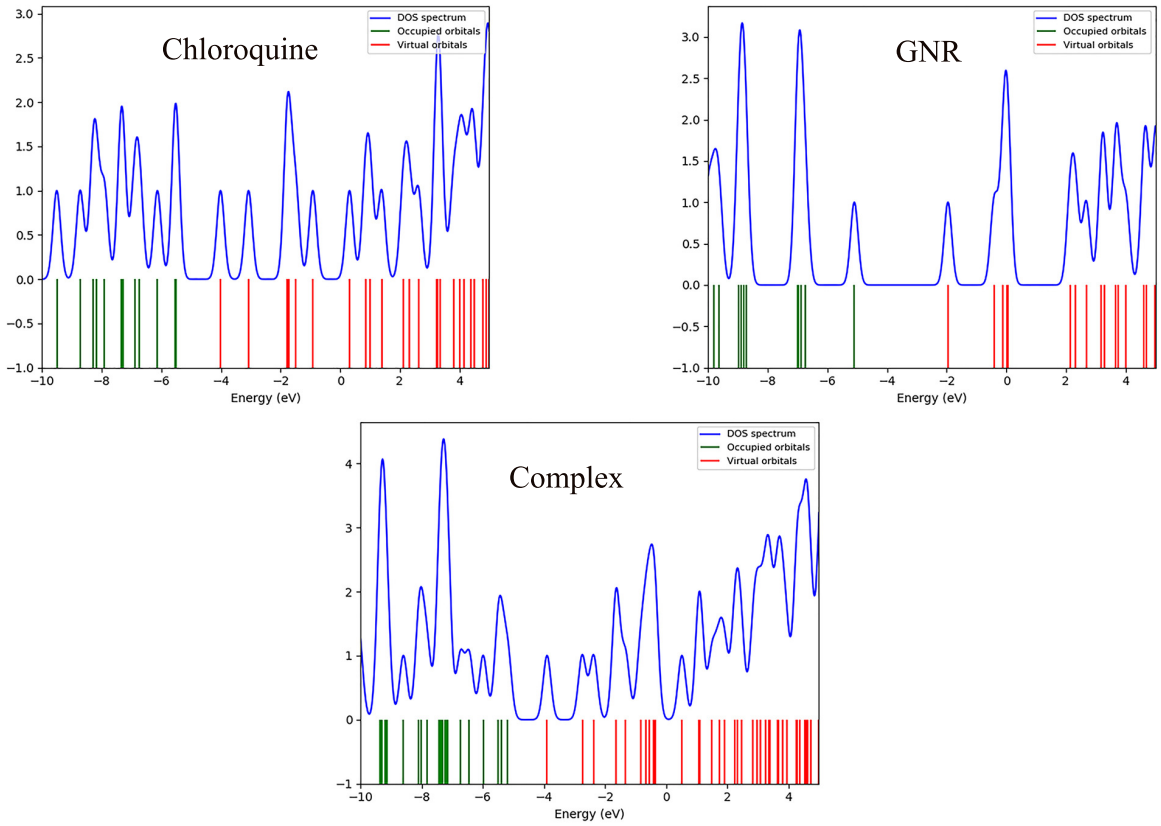

Figure 2. The dependence of density of states versus incident electron energy for GNR, chloroquine and chloroquine-GNR complex.

Atoms	Chloroquine-GNR
$C_{61}-H_{25}$	3.15
$C_{34}-H_{28}$	2.97
$H_{28}-H_{52}$	3.50
$C_{33}-H_{28}$	2.74
$C_{35}-H_{25}$	2.85

Table 2. The bond length of the chloroquine-GNR atoms.

Nanostructures	E_{HOMO}(eV)	E_{LUMO}(eV)	E_{gap}(eV)	E_F(eV)	Dipole M (Debye)
GNR	-5.1	-1.96	3.14	3.53	0
Chloroquine	-5.5	-4.01	1.49	4.75	12.29
Chloroquine-GNR	-5.18	-3.9	1.28	4.54	13.43

Table 3. Electronic properties of the chloroquine, GNR and chloroquine and GNR complex.

Our calculations for E_{LUMO}, E_{HOMO}, energy gap, Fermi energy and dipole moment are reported in Table 3. Table 3 shows that the energy gap for GNR and chloroquine are 3.14 (eV) and 1.48 (eV) respectively that is more for GNR than the drug. Also, the energy gap of the chloroquine-GNR complex is 1.28 (eV), which is reduced compared to GNR and drug separately. It is clear that the dipole moment for the drug is much higher than that of GNR. The dipole moment has increased in the case of the chloroquine-GNR complex compared to chloroquine and GNR separately.

The LUMO and HOMO orbitals for chloroquine-GNR complex are shown in Figure 3. It is observed that the population of LUMO and HOMO orbitals are in $(RS)-N'-(7-chloroquinolin-4-yl)-pentane-1-amine$ and N-terminal, respectively.

2.2 Stability properties

In this section, we obtained the infrared spectra (IR) and UV-Vis spectrums of the GNR, chloroquine and chloroquine-GNR complex, and to determine their stability, we drew the real part of the frequency vibrations[47]. Figure 4 shows the IR spectrum for GNR, chloroquine and chloroquine-GNR complex. The IR spectrum includes parameters such as frequency, ε (wave energy levels) and dipole strength (D). Absorption for GNR, chloroquine and the complex occurs in the range of 500-3000 (cm^{-1}), 500-2300 (cm^{-1}) and 500-2300 (cm^{-1}) respectively. Also, the maximum vibrational frequency for GNR, chloroquine and complex occurs in 840 (cm^{-1}), 703.76 (cm^{-1}) and 700 (cm^{-1}) respectively. Therefore, as the GNR and drug are combined, the maximum vibration frequency is reduced. Figure 5 shows the UV-Vis spectrums of the incident parameters versus the wavelength, ε and oscillator strength for GNR, chloroquine and chloroquine-GNR complex. In UV-Vis spectrums the absorption index for GNR, chloroquine and complex are in the range of 283-585 (nm), 584-3000 (nm) and 688-2536 (nm) respectively. The maximum vibration frequency for GNR, chloroquine and complexes occur in 411 (nm), 1235 (nm) and 1024 (nm) respectively.

2.3 Electrochemical properties

Here, we study the electrochemical properties of GNR, chloroquine and chloroquine-GNR complex. The parameters investigated include the chemical potential (μ), chemical hardness (η), global softness (S) and electrophilicity index (ω) which are listed in Table 4. Chemical potential calculations show that the chloroquine drug is more negative than GNR. Both values of the ionization energy (IP) and electron affinity (EA) are positive. Also, ionization energy and electron affinity are more negative for the drug than GNR due to the fact that HOMO and LUMO levels are more negative. According to Table 4, the chemical hardness for chloroquine is smaller than the GNR due to the small difference between the levels of LUMO and HOMO. Because the chemical hardness values for GNR are higher than those for the drug, the global softness for GNR is smaller compared to the chloroquine. It is observed that the electrophilicity index for chloroquine drug is more stronger than that of GNR. The reason for this increase in the drug is the large amount of chemical potential. We see that in the chloroquine-GNR complex, other parameters are reduced except for global softness and electrophilicity index. In other words, amount of global softness and electrophilicity for the chloroquine-GNR complex has increased compared to the drug and GNR separately. Using Eq. (7), the GNR absorption values in chloroquine drug are obtained as 7.9 (kj/mol) or 1.88 ($kcal/mol$). GNR is absorbed in chloroquine due to its positive absorption values.

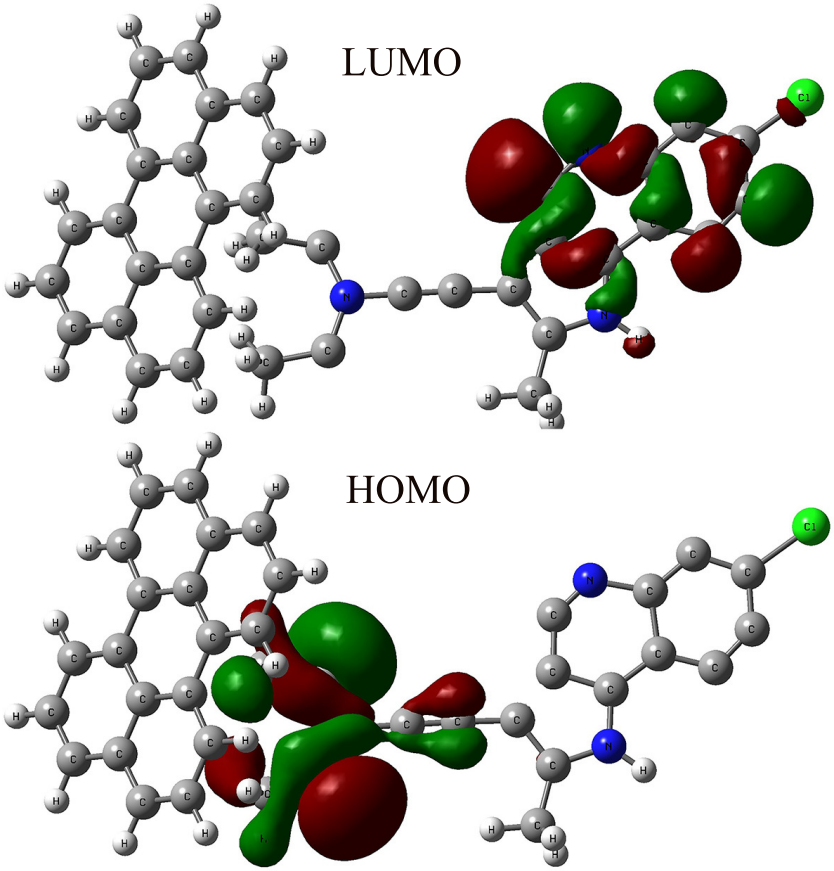

Figure 3. The schematic of HOMO and LUMO orbitals for chloroquine-GNR complex.

Nanostructures	μ	IP	EA	η	S	ω
GNR	-3.53	5.1	1.96	1.57	0.63	3.96
Chloroquine	-4.75	5.5	4.01	0.74	1.35	15.24
Chloroquine-GNR	-4.54	5.18	3.9	0.64	1.56	16.10

Table 4. Electrochemical properties of the introduced chloroquine, GNR and chloroquine-GNR complex.

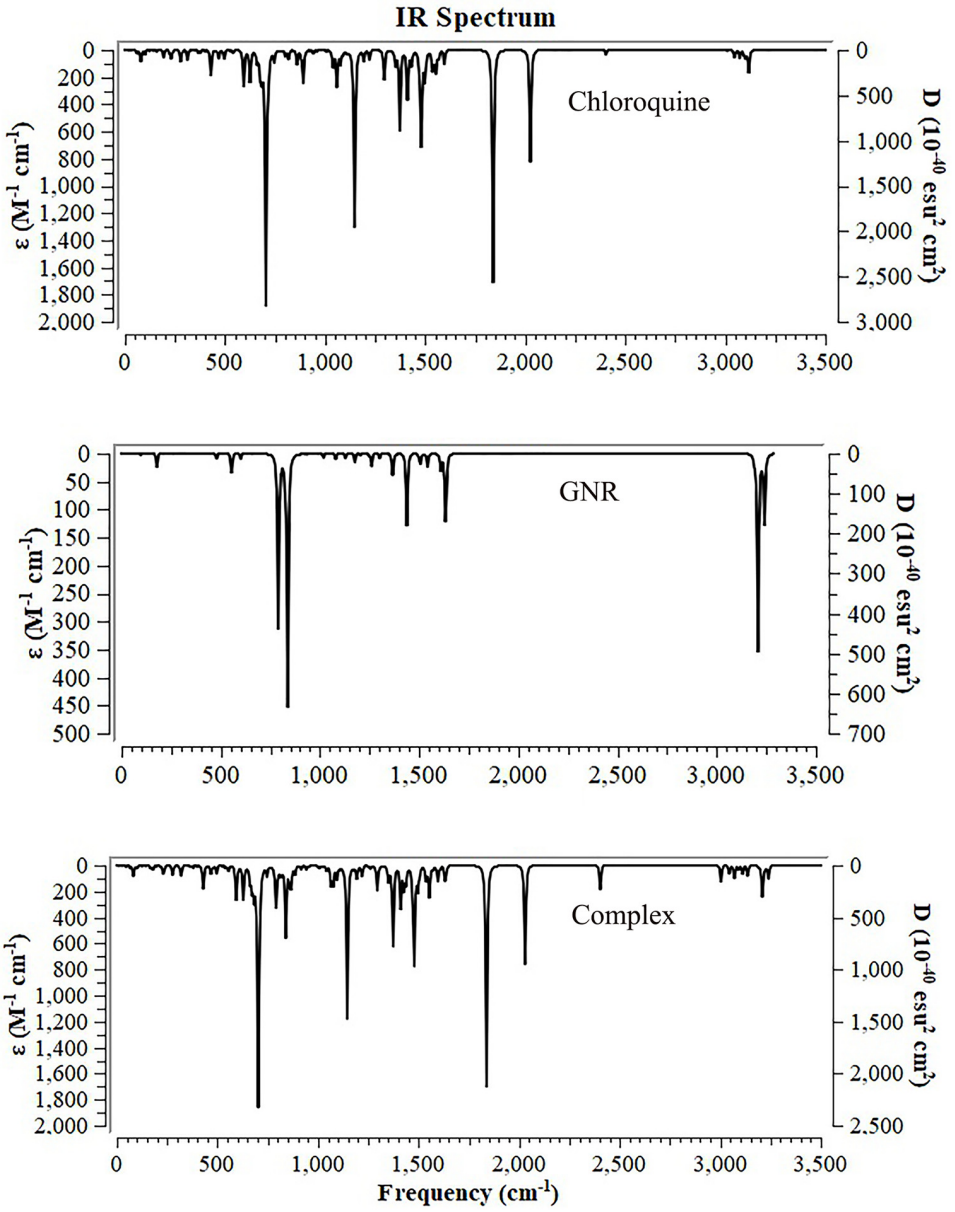

Figure 4. The infrared spectrums of the incident parameters versus the frequency, ε and dipole strength (D) for GNR, chloroquine drug and chloroquine-GNR complex.

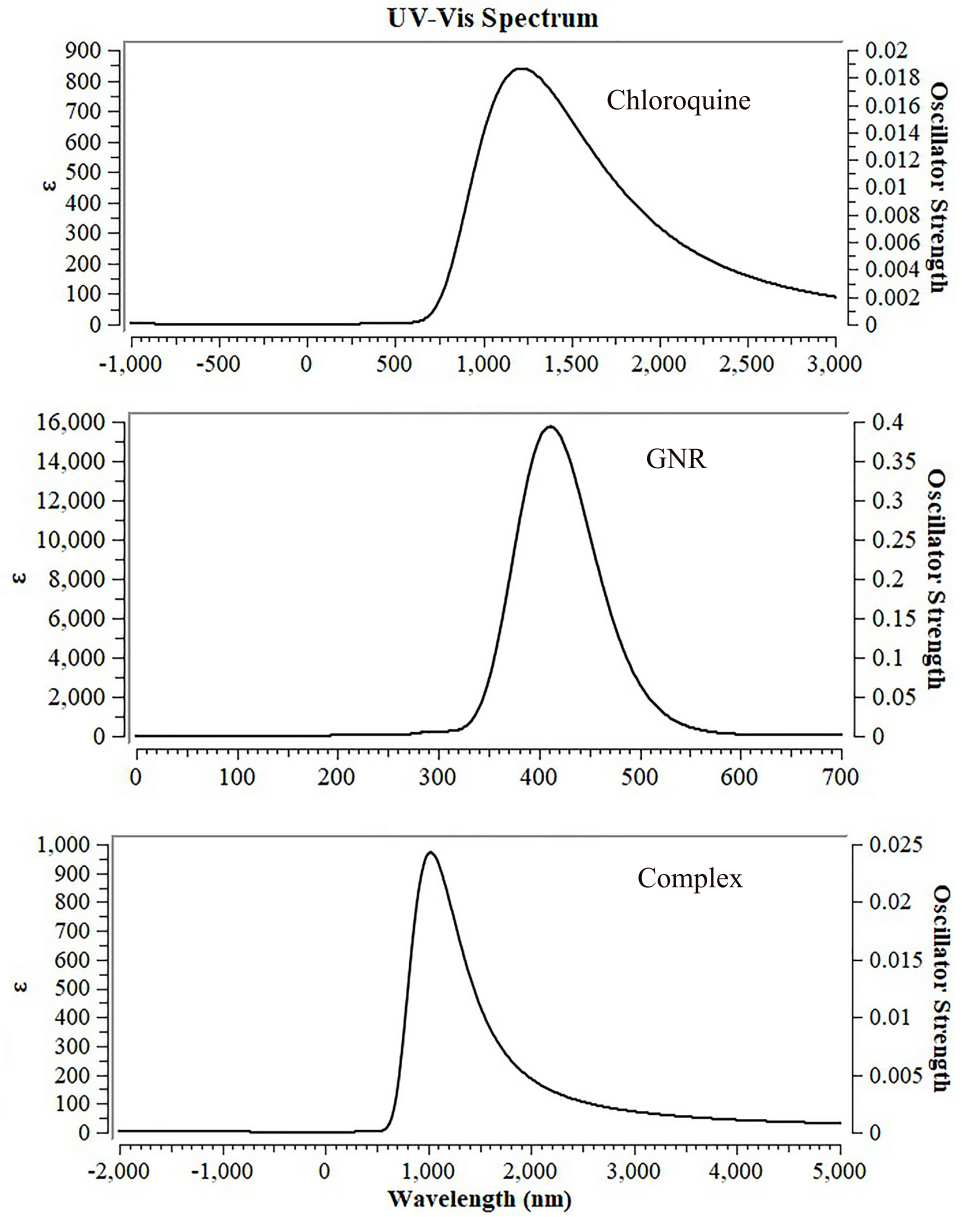

Figure 5. The UV-Vis spectrums of the incident parameters versus the wavelength, ε and oscillator strength for GNR, chloroquine and chloroquine-GNR complex.

3 Conclusion

Using the DFT method, we numerically evaluated the electrical, structural, and adsorption properties for optimized graphene nanoribbon (GNR), chloroquine, and chloroquine-GNR complex nanostructures. The density of state calculations illustrate that the energy gap for the chloroquine-GNR complex is reduced relative to the GNR and drug, and the electron conductance is increased. Our results show that parameters such as dipole moment, global softness and electrophilicity increase with the formation of complex. Examination of the infrared spectra and UV-Vis spectrums of the absorption spectra indicates that GNR is absorbed in the chloroquine drug. We have shown that GNR nanostructures are suitable for complexes with chloroquine drug and can be very effective in the drug delivery of chloroquine and therefore help treat COVID-19.

4 Acknowledgements

This research has been supported by Azarbaijan Shahid Madani University. We are also grateful to Jaber Jahanbin Sardroodi and Samaneh Baranipur for granting their knowledge. Competing interests: The authors declare no competing interests.

References

1. Zhavoronkov, A. et al. Potential 2019-nCoV 3C-like protease inhibitors designed using generative deep learning approaches. *Chem. Rxiv. TM*. doi.org/10.26434/chemrxiv.11829102.v2. (2020).
2. Guo, Y. R. et al. The origin, transmission and clinical therapies on coronavirus disease 2019 (COVID-19) outbreak- an update on the status. *Military Med. Res.* **7**, 11 (2020).
3. Ahmed, S. F. et al. Preliminary Identification of Potential Vaccine Targets for the COVID-19 Coronavirus (SARS-CoV-2) Based on SARS-CoV Immunological Studies. *Viruses* **12**, 254 (2020).
4. Chan, J. F. W. et al. Middle east respiratoty syndrome coronavirus: another zoonotic betacoronavirus causing SARS-like disease. *Clin. Microbiol. Rev.* **28**, 465-522 (2015).
5. Hui, D. S. et al. The continuing 2019-nCoV epidemic threat of novel coronaviruses to global health - the latest 2019 novel coronavirus outbreak in Wuhan, China. *Int. J. Infect. Dis.* **91**, 264-6 (2020).
6. Bogoch, I. I. et al. Potential for global spread of a novel coronavirus from China. *J. Travel. Med.* **27**, 1-3 (2020).
7. World Health Organization. Infection prevention and control during health care when COVID-19 is suspected https://www.who.int/publications-detail/infection-prevention-and-control-during-health-care-when-novel-coronavirus-(ncov)-infection-is-suspected-20200125.
8. Touret, F. et al. Commentary Of chloroquine and COVID-19. *Antivir. Res.* **177**, 104762 (2020).
9. Colson, Ph. et al. Chloroquine for the 2019 novel coronavirus. *Int. J. Antimicrob. Agents.* **55**, 105923 (2020).
10. Colson, Ph. et al. Chloroquine and hydroxychloroquine as available weapons to fight COVID-19. *Int. J. Antimicrob. Agents.* doi: https://doi.org/10.1016/j.ijantimicag.2020.105932 (2020).
11. Gao, j. et al. Breakthrough: Chloroquine phosphate has shown apparent efficacy in treatment of COVID-19 associated pneumonia in clinical studies. *Biosci. Trends* **14**, 72-3 (2020).
12. Sa, J. M. et al. Plasmodium vivax chloroquine resistance links to pvcrt transcription in a genetic cross. *Nat. Commun.* **10**, 4300 (2019).
13. Smolen, J. S. et al. EULAR recommendations for the management of rheumatoid arthritis with synthetic and biological disease- modifying antirheumatic drugs: 2013 update. *Ann. Rheum. Dis*. **73**, 492-509 (2014).
14. Fanouriakis, A. et al. 2019 update of the EULAR recommendations for the management of systemic lupus erythematosus. *Ann. Rheum. Dis.* **78**, 736-45 (2019).
15. Pons- Estel, B. A. et al. First Latin American clinical practice guidelines for the treatment of systemic lupus erythematosus: Latin American Group for the Study of Lupus (GLADEL, Grupo Latino Americano de Estudio del Lupus)-Pan- American League of Associations of Rheumatology (PANLAR). *Ann. Rheum. Dis.*, **77**, 1549-57 (2018).
16. Gordon, C. et al. The British Society for Rheumatology guideline for the management of systemic lupus erythematosus in adults. *Rheumatology* **57**, e1-e45 (2018).
17. Tektonidou, M. G. et al. EULAR recommendations for the management of antiphospholipid syndrome in adults. *Ann. Rheum. Dis.* **78**, 1296-1304 (2019).
18. Vivino, F. B. et al. New treatment guidelines for Sjogren's disease. *Dis. Clin. North. Am.* **42**, 531-51 (2016).

19. Tsai, W. P. et al. Inhibition of human immunodeficiency virus infectivity by chloroquine. *AIDS Res. Hum. Retrovir.* **6**, 481-9 (1990).

20. Li, C.; Zhu, X. et al. Chloroquine, a FDA-approved drug, prevents Zika virus infection and its associated congenital microcephaly in mice. *EBioMedicine* **24**, 189-94 (2017).

21. Delvecchio, R. et al. Chloroquine, an Endocytosis Blocking Agent, Inhibits Zika Virus Infection in Different Cell Models. *Viruses* **8**, 322 (2016).

22. Sweiti, H. et al. Repurposed therapeutic agents targeting the Ebola virus: a systematic review. *Curr. Ther. Res. Clin. Exp.* **84**, 10-21 (2017).

23. Diaz-Griffero, F. et al. Endocytosis is a critical step in entry of subgroup Bavian leukosis viruses. *J. Virol.* **76**, 12866-76 (2000).

24. Byrd, T. F. et al. Chloroquine inhibits the intracellular multiplication of Legionella pneumophila by limiting the availability of iron. A potential new mechanism for the therapeutic effect of chloroquine against intracellular pathogens. *J. Clin. Invest.* **88**, 351-7 (1991).

25. Legssyer, R. et al. Changes in function of iron-loaded alveolar macrophages after in vivo administration of desferrioxamine and/or chloroquine. *J. Inorg. Biochem.* **94**, 36-42 (2003).

26. Tyagi, N. et al. Recent progress on biocompatible nanocarrier-based genistein delivery systems in cancer therapy. *J. Drug Target*. **27**, 394-407 (2019).

27. Zhao, J. et al. Smart nanocarrier based on PEGylated hyaluronic acid for deacetyl mycoepoxydience: high stability with enhanced bioavailability and efficiency. *Carbohydrate Polymers* **203**, 356-68 (2019).

28. Borandeh, S. et al. structural and in-vitro characterization of β -cyclodextrin grafted L-phenylalanine functionalized graphene oxide nanocomposite: a versatile nanocarrier for pH-sensitive doxorubicin delivery. *Carbohydrate Polymers* **201**, 151-61 (2018).

29. Li, Z; Tian, L. et al. Graphene oxide/ag nanoparticles cooperated with simvastatin as a high sensitive X-ray computed tomography imaging agent for diagnosis of renal dysfunctions. *Adv. Healthcare Material.* **6**, 18 (2017).

30. Wang, C. et al. A magnetic and pH-sensitive composite nanoparticle for drug delivery. *J. Colloid and Inter. Sci.* **516**, 332-41 (2018).

31. Kozik, V. et al. Derivatives of graphene oxide as potential drug carriers. *J. Nanosci. Nanotechnol.* **19**, 2489-92 (2019).

32. Youn, H. et al. Aptasensor for multiplex detection of antibiotics based on FRET strategy combined with aptamer/ graphene oxide complex. *Scientific Reports* **9**, 7659 (2019).

33. Ye, Y. et al. Functional Graphene Oxide Nanocarriers for Drug Delivery. *Int. J. Polymer Sci.* **7**, 8453493 (2019).

34. Ghawanmeh, A. A. et al. Graphene oxide-based hydrogels as a nanocarrier for anticancer drug delivery. *Nano Res.* **12**, 973-90 (2019).

35. Iannazzo, D. et al. Smart Nanovector for Cancer Targeted Drug Delivery Based on Graphene Quantum Dots. *Nanomaterial*. **9**, 282 (2019).

36. Cakmak, N. K. et al. Synthesis and stability analysis of folic acid-graphene oxide nanoparticles for drug delivery and targeted cancer therapies. *Int. Adv. Res. Eng. J.* **3**, 081-5 (2019).

37. Campbell, E. et al. Graphene Oxide as a Multifunctional Platform for Intracellular Delivery, Imaging, and Cancer Sensing. *Scientific Reports* **9**, 416 (2019).

38. Frisch, M. J. et al. Revision A.1, Gaussian. *Inc. Wallingford CT.* (2009).

39. Lee, C. et al. Density-Functional Crystal Orbital Study on the Structures and Energetics of Polyacetylene Isomers. *Phys. Rev. B.* **37**, 785-9 (1988).

40. Becke, A. D. Density-Functional Thermochemist1ry. III. The Role of Exact Exchange. *J. Chem. Phys.* **98**, 5648-52 (1993).

41. Melvin, E. et al. Iconography: the remarkable ability of B3LYP/3-21G(*) calculations to describe geometry, spectral and electrochemical properties of molecular and supramolecular porphyrinefullerene conjugates. *Elsevier Masson* **9**, 960-81 (2006).

42. Lu, X. et al. Are Stone-Wales defect sites always more reactive than perfect sites in the sidewalls of single-wall carbon nanotubes. *J. Am. Chem. Soc.* **127**, 20-1 (2005).

43. Beheshtian, J. et al. Induced polarization and electronic properties of carbon doped boron-nitride nanoribbons. *Phys. Rev. B.* **86**, 195433 (2012).

44. Wang, T. et al. The electronic properties of chiral silicon nanotubes. *Superlattice. Microst.* **109**, 1-6 (2017).

45. Tavakol, H.; Shahabi, D. DFT, QTAIM, and NBO study of adsorption of rare gases into and on the surface of sulfur-doped, single-wall carbon nanotubes. *J. Phys. Chem. C.* **119**, 6502-10 (2015).

46. Zhang, Q. et al. Lithium Insertion In Silicon Nanowires: An ab Initio Study. *Nano Lett.* **10**, 3243-9 (2010).

47. Li, J. et al. Density functional theory studies of $Si_{36}H_{36}$ and $C_{36}H_{36}$ nanocages. *Int. J. Quantum Chem.* **5**, 725-30 (2014).

Figures

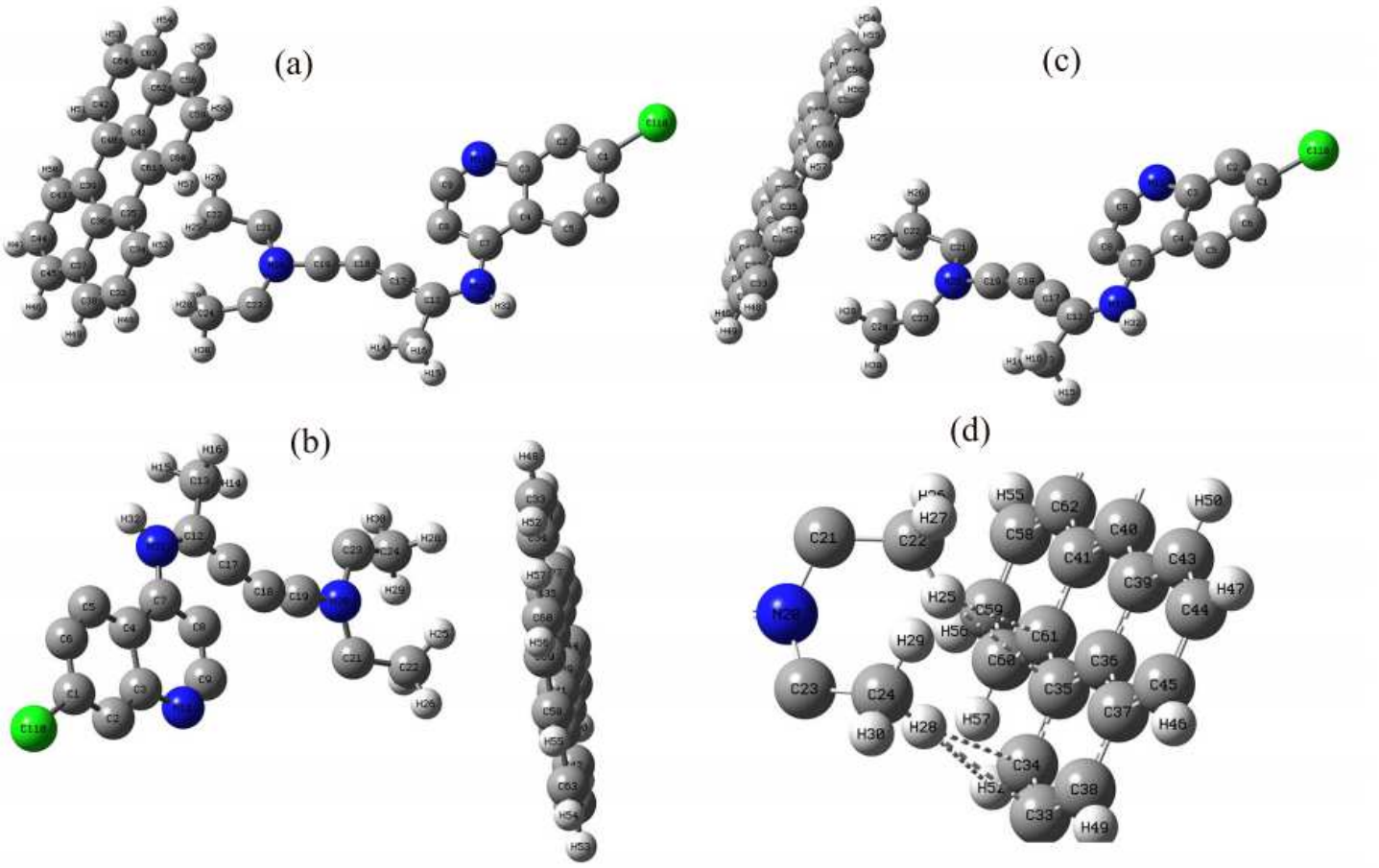

Figure 1

Three-dimensional view of the complex of chloroquine and GNR from different views (the sharp of (a), (b) and (c)) and the part of intraction between chloroquine and GNR (d).

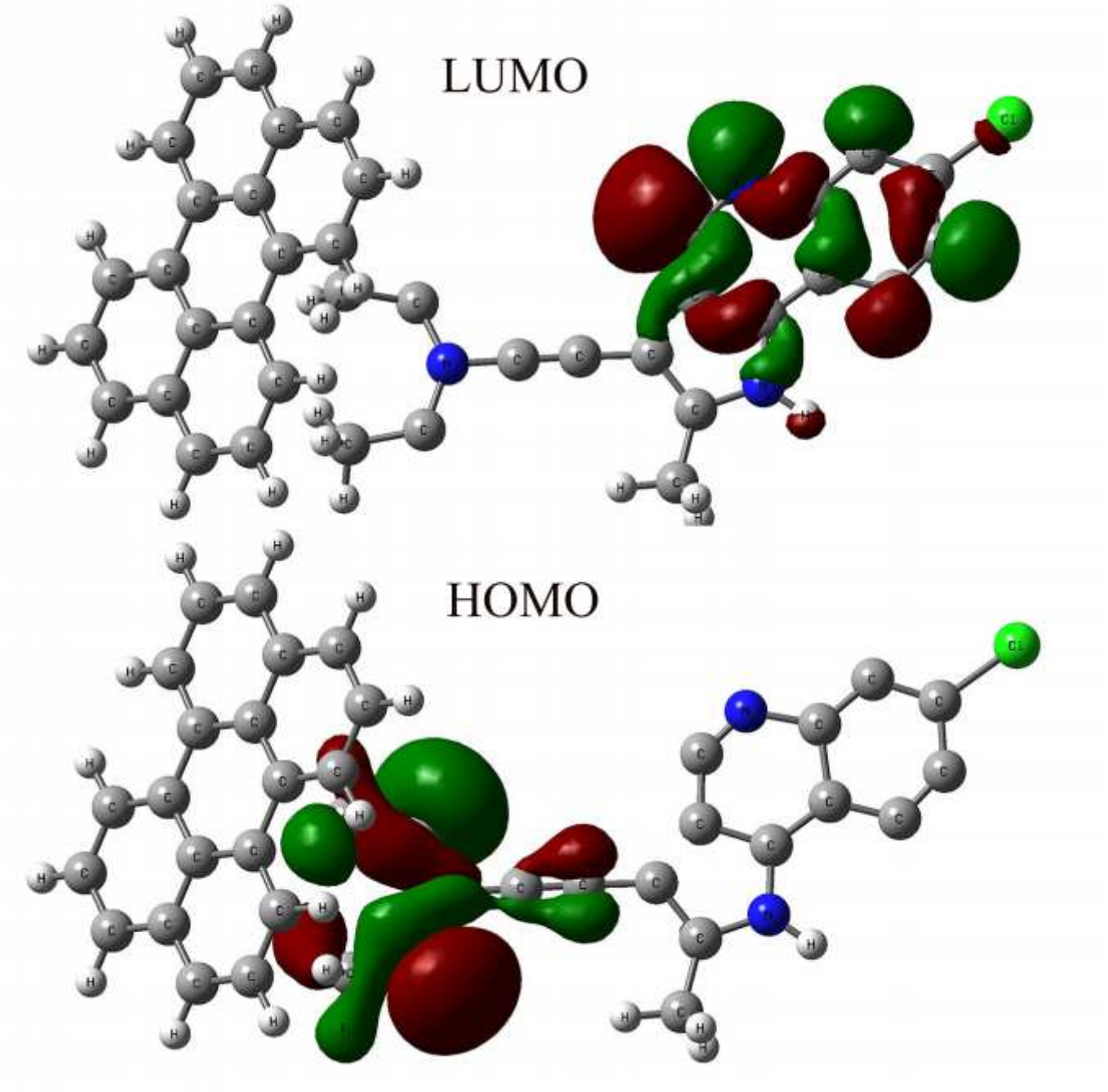

Figure 2

The dependence of density of states versus incident electron energy for GNR, chloroquine and chloroquine-GNR complex.

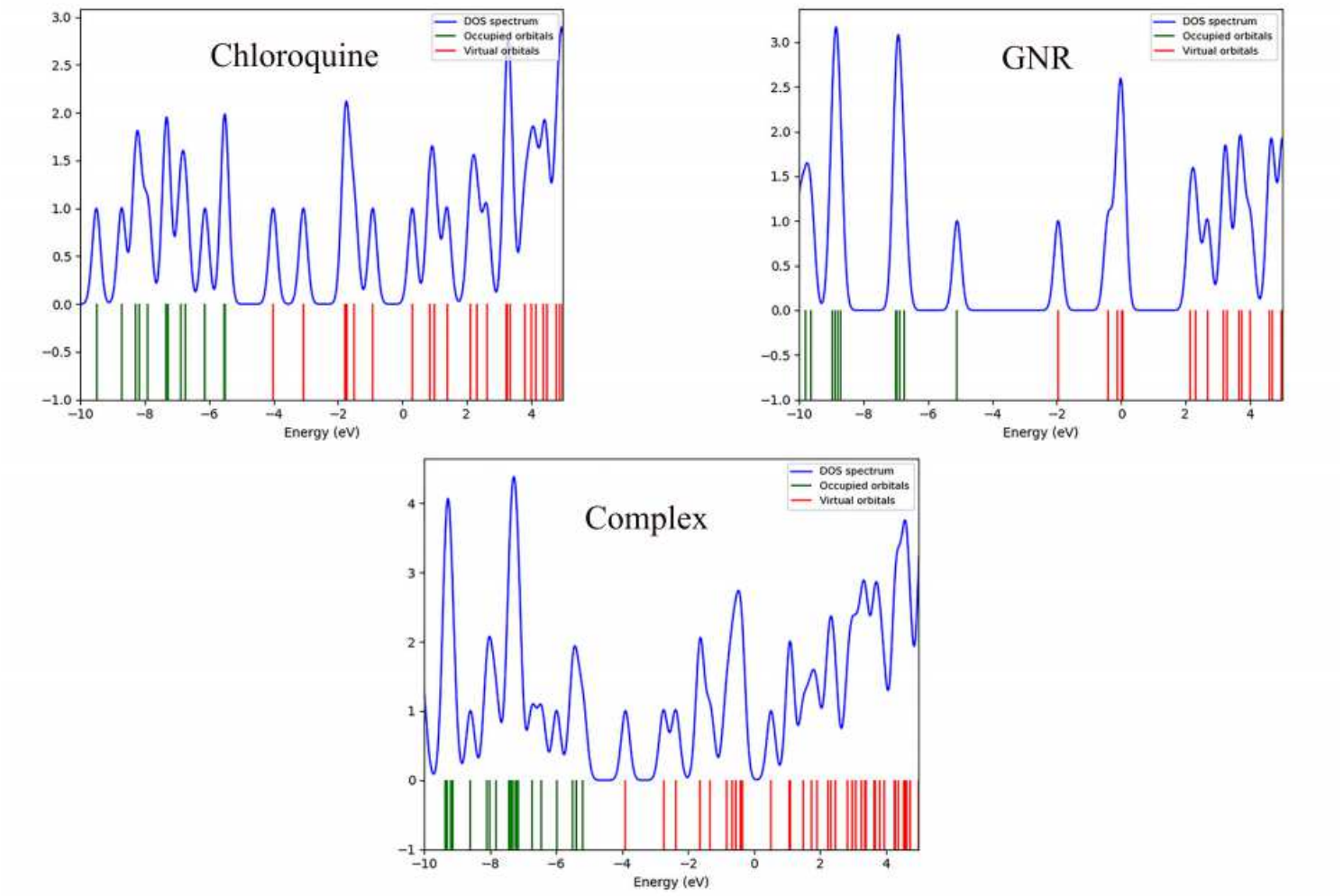

Figure 3

The schematic of HOMO and LUMO orbitals for chloroquine-GNR complex.

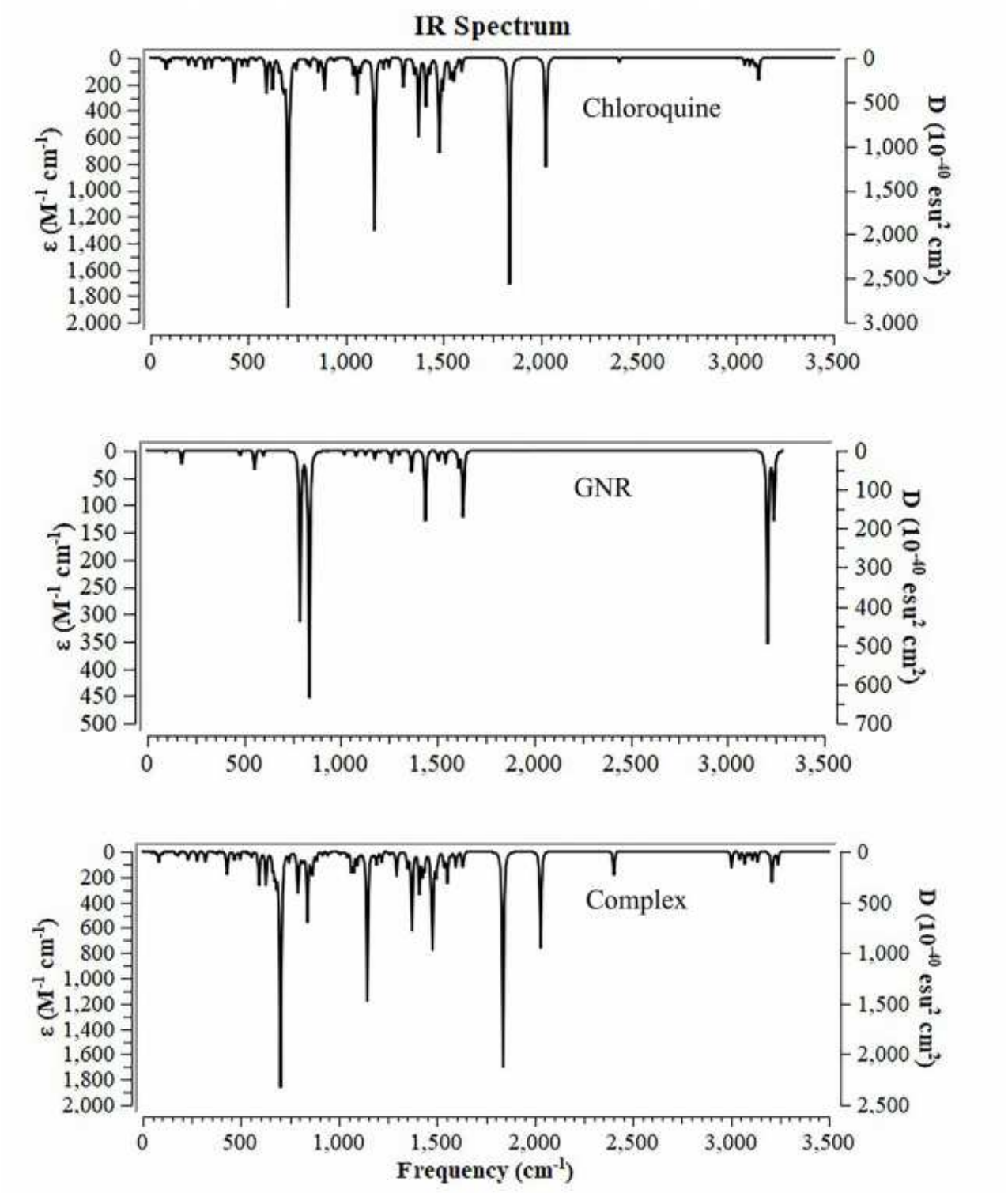

Figure 4

The infrared spectrums of the incident parameters versus the frequency, ε and dipole strength (D) for GNR, chloroquine drug and chloroquine-GNR complex.

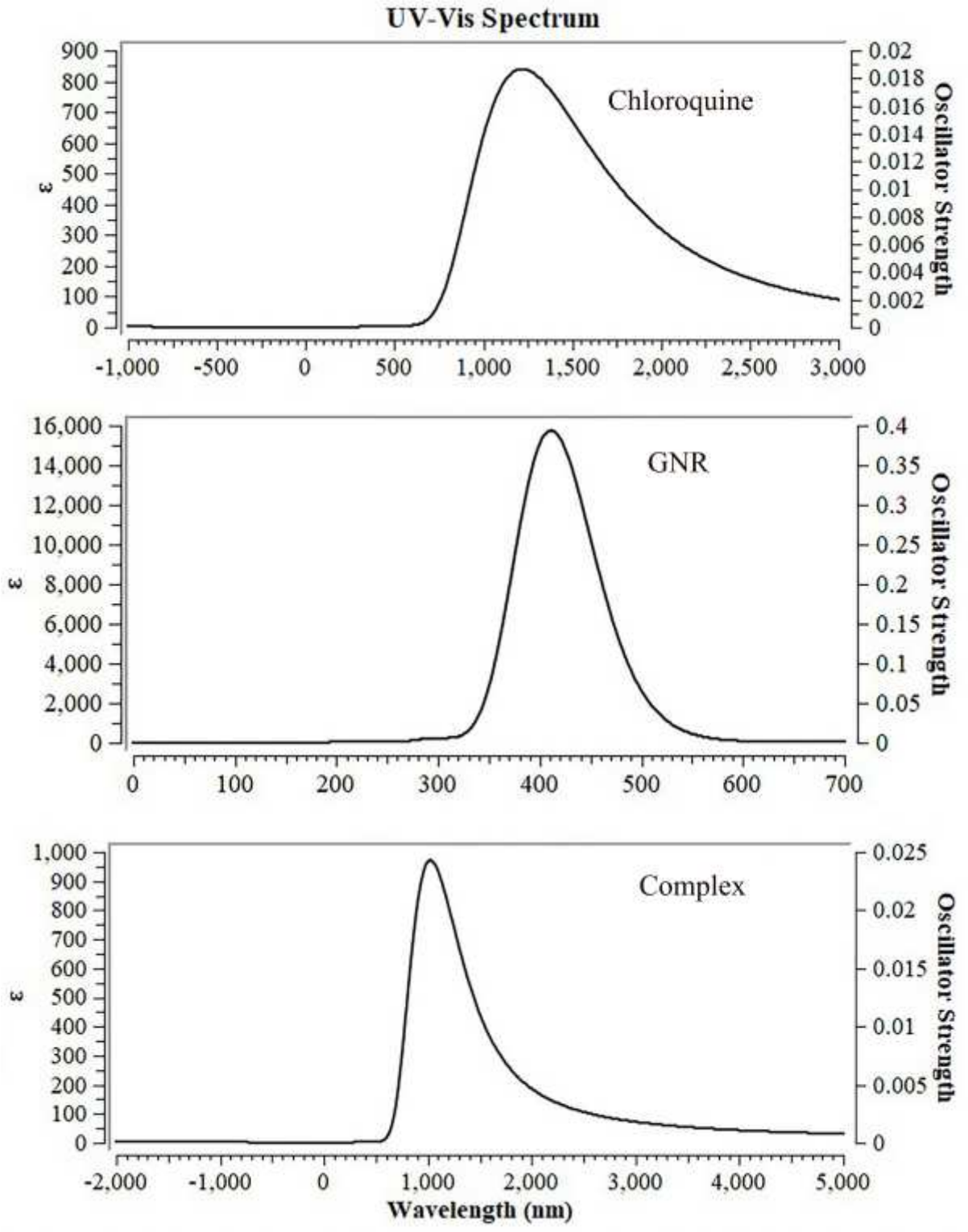

Figure 5

The UV-Vis spectrums of the incident parameters versus the wavelength, ε and oscillator strength for GNR, chloroquine and chloroquine-GNR complex.